Using beamforming to maximise the detection capability of small, sparse seismometer arrays deployed to monitor oil field activities

James P. Verdon[1,2*], J.-Michael Kendall[1,2], Stephen P. Hicks[3] and Philip Hill[3]

[1]*School of Earth Sciences, Wills Memorial Building, University of Bristol, Queen's Road, Bristol, BS8 1RJ, UK,* [2]*Outer Limits Geophysics LLP, 608 Malt House, East Tucker Street, Bristol, BS1 6LQ, UK, and* [3]*Güralp Systems Ltd., Midas House, Calleva Park, Aldermaston, Reading RG7 8EA, UK*

ABSTRACT

Like most other industrial activities that affect the subsurface, hydraulic fracturing carries the risk of reactivating pre-existing faults and thereby causing induced seismicity. In some regions, regulators have responded to this risk by imposing traffic light scheme-type regulations, where fracture stimulation programs must be amended or shut down if events larger than a given magnitude are induced. Some sites may be monitored with downhole arrays and/or dense near-surface arrays, capable of detecting very small microseismic events. However, such monitoring arrangements will not be logistically or economically feasible at all sites. Instead, operators are using small, sparse arrays of surface seismometers to meet their monitoring obligations.

The challenge we address in this paper is to maximise the detection thresholds of such small, sparse, surface arrays so that they are capable of robustly identifying small-magnitude events whose signal-to-noise ratios may be close to 1. To do this, we develop a beamforming-and-stacking approach, computing running short-term/long-term average functions for each component of each recorded trace (P, S_H, and S_V), time-shifting these functions by the expected travel times for a given location, and performing a stack.

We assess the effectiveness of this approach with a case study using data from a small surface array that recorded a multi-well, multi-stage hydraulic fracture stimulation in Oklahoma over a period of 8 days. As a comparison, we initially used a conventional event-detection algorithm to identify events, finding a total of 17 events. In contrast, the beamforming-and-stacking approach identified a total of 155 events during this period (including the 17 events detected by the conventional method). The events that were not detected by the conventional algorithm had low-signal-to-noise ratios to the extent that, in some cases, they would be unlikely to be identified even by manual analysis of the seismograms. We conclude that this approach is capable of improving the detection thresholds of small, sparse arrays and thus can be used to maximise the information generated when deployed to monitor industrial sites.

1 INTRODUCTION

Over the past 15 years, the use of hydraulic fracturing to extract hydrocarbons from shale and other low-permeability rocks has seen substantial growth. Wang and Krupnick (2013) provide a useful history describing how hydraulic fracturing, a well-established technique used in conventional reservoirs for 65 years, came to be used to extract gas from shale rocks. Hydraulic fracturing intentionally generates new fracture networks in the target rocks. This fracturing is accompanied by

*E-mail: James.Verdon@bristol.ac.uk

microseismic activity, i.e., very small seismic events that can be detected only using specialised monitoring arrays.

However, in a number of cases, the stress and pressure changes induced by hydraulic fracturing have been sufficient to reactivate pre-existing critically stressed faults, producing larger earthquakes of sufficient magnitude to be felt by local populations (e.g., BC Oil and Gas Commission 2012, 2014; Clarke *et al.* 2014; Friberg, Besana-Ostman and Dricker 2014; Darold *et al.* 2014; Skoumal, Brudzinski and Currie 2015; Schulz *et al.* 2015; see summary by Verdon and Kendall (2015)).

Given the very large number of hydraulic stimulations performed around the world, instances of felt seismic events are very rare and can be compared favourably with respect to many other industrial activities such as hydroelectric reservoir impoundment, coal mining, geothermal energy extraction, and deep re-injection of wastewater (National Research Council 2013). Nevertheless, in some jurisdictions, legislators have responded by imposing traffic light scheme (TLS) regulations that require operators to cease their activities if earthquakes above a given magnitude are deemed to have been induced by hydraulic fracturing.

For example, in Alberta and British Columbia, Canada, an amber warning is issued if events exceed $M_L = 2.0$, and operations must be stopped if events exceed $M_L = 4.0$. In Ohio, where hydraulic fracturing is conducted within 3 miles of a known seismogenic fault, operations must be paused if an event larger than $M_L = 1.0$ is detected. The UK government has mandated a TLS such that, if hydraulic fracturing induces an event larger than $M_L = 0.0$, then flowback periods must be extended and injection volumes used for future stages (amber status) must be reduced, whereas if stimulation induces events larger than $M_L = 0.5$, then injection must cease immediately (Green, Styles and Baptie 2012).

Small-magnitude induced events can be monitored using downhole geophone arrays (e.g., Maxwell *et al.* 2010) or by very large and very dense (typically >1000 stations) surface arrays (e.g., Chambers *et al.* 2010a). These arrays can detect very small events, which are used to map the hydraulic fractures. However, such arrays can be expensive to deploy and may not be logistically feasible at many sites. Generally speaking, most operators will not deploy such arrays at every site. Instead, in response to new injection-induced seismicity regulations, operators of shale gas sites (and of other types of operation thought to be prone to induced seismicity) are beginning to deploy small (10–20 stations) networks of portable surface seismometers in order to monitor induced seismicity. These arrays are relatively inexpensive, flexible, and easily
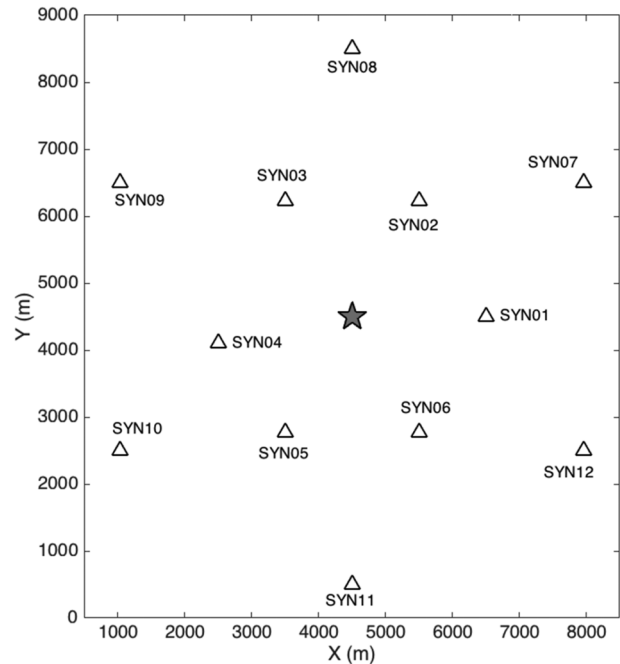

Figure 1 (Triangles) Receiver positions and (grey star) event position used for the synthetic model. The event is modelled at a depth of 3500 m.

Table 1 One-dimensional layered velocity model used to generate the synthetic model

Depth to layer top (m)	V_P (m/s)	V_S (m/s)
0	1300	765
100	2000	1176
250	2400	1412
500	2700	1588
1000	2900	1706
1500	3200	1882
2000	3500	2059
2500	3800	2235
3000	4100	2412
3500	4300	2529
4000	4500	2647

deployed (from a logistical perspective), making them an attractive proposition where regulations mandate monitoring at every operational site.

Given the expected deployment of small, sparse, surface arrays at future shale gas sites (and other sites prone to injection-induced seismicity), the challenge we address in this paper is to develop methods that improve detection

thresholds for such arrays, bearing in mind that seismic noise levels around shale gas sites may often be quite high.

Our motivation for doing so is twofold.

- In the general case, by improving detection thresholds and thereby detecting more smaller events, an operator will have more information with which to inform their stimulation program.

- In the specific case, we concern ourselves with the UK's TLS, where operators must be able to guarantee detection thresholds lower than $M_L = 0.0$ (Green *et al.* 2012). Although the UK is generally considered to be a quiet place in terms of seismicity, it is not quiet in terms of seismic noise. This noise may be both anthropogenic (e.g., roads, railways, industrial, and agricultural activities) and natural (e.g., wind and waves). Therefore, achieving detection thresholds lower than $M_L = 0.0$ with an array of surface seismometers may be challenging (e.g., Horleston *et al.* 2013).

Commonly, earthquakes are detected using automated picking algorithms that identify changes in energy and/or frequency content of the recorded traces (Lomax, Satriano and Vassallo 2012), with the additional constraint that such triggers be identified on multiple stations of a network within a specified time window.

However, alternative event detection methods based on delay-and-stack methods are also available (also referred to as beamforming or focusing imaging). Based on expected phase arrival times from a given subsurface point, traces are time-shifted such that coherent phase arrivals will be aligned. When stacked, these coherent arrivals interfere constructively, boosting the signal, whereas incoherent noise interferes destructively, reducing the noise. The net result is an improvement in signal-to-noise ratios such that small events with low-signal-to-noise ratios can be detected even where no clear arrival is visible or pickable on individual traces.

The ability of such beamforming (or delay-and-stack) methods to detect smaller-magnitude events, with signal-to-noise ratios much less than 1, was demonstrated for large and dense arrays (e.g., Chambers *et al.* 2010a; Duncan and Eisner 2010). In this paper, we adapt such a method for use with data from small surface arrays as might be deployed to monitor induced seismicity around industrial sites. However, rather than stacking the raw waveforms as per Chambers *et al.* (2010a), we use a method that is more similar to that proposed by Grigoli *et al.* (2014), who stack functions based on running short- and long-term averages of trace characteristic functions. Furthermore, while Chambers *et al.* (2010a)

use only P–wave arrivals and Grigoli *et al.* (2014) use P–waves and a single combined S–wave arrival, in this study, we utilise a method that combines stacks of both P, S_H, and S_V phases.

Our primary aim is to assess whether such methods are capable of detecting and locating events that would be missed by the more commonly used event detection algorithms that are based on automated phase picking algorithms. To do so, we apply this approach to data recorded during hydraulic fracturing of a well in Oklahoma. Whereas Grigoli *et al.* (2014) examined the capability of a short-term/long-term average ratio stacking algorithm to relocate events more accurately (events with a reasonably high-signal-to-noise ratio that had already been identified with conventional automatic picking), in this study, we seek to compare the event detection capabilities of such an algorithm to determine whether this approach is capable of detecting events that would be missed by conventional automatic phase picking algorithms.

2 METHOD

2.1 Beamforming and stacking

We begin by generating both P– and S–wave travel-time lookup tables from candidate event locations to each receiver. Shale rocks are usually very anisotropic (e.g., Kendall *et al.* 2007), and recent studies have shown that vertical transverse isotropic (VTI) anisotropic velocity models are often necessary to accurately image microseismic events recorded in shale basins using surface arrays (e.g., Eisner *et al.* 2011; Grechka 2015). We therefore develop a method that is capable of incorporating VTI anisotropic velocity models where necessary. We therefore compute travel times for P, S_H, and S_V phases ($t_P(\mathbf{x}, n)$, $t_{SH}(\mathbf{x}, n)$, and $t_{SV}(\mathbf{x}, n)$) for each receiver n, where $\mathbf{x}$ is a potential source location coordinate. A range of methods are available for computing travel times in anisotropic media (e.g., Guest and Kendall 1993; Fomel 2004).

From these travel-time tables, we compute the arrival times across the array relative to the first P–wave arrival at any receiver:

$$dt_P(\mathbf{x}, n) = t_P(\mathbf{x}, n) - \min(t_P(\mathbf{x})),$$
$$dt_{S_H}(\mathbf{x}, n) = t_{S_H}(\mathbf{x}, n) - \min(t_P(\mathbf{x})), \qquad (1)$$
$$dt_{S_V}(\mathbf{x}, n) = t_{S_V}(\mathbf{x}, n) - \min(t_P(\mathbf{x})),$$

where $\min(t_P(\mathbf{x}))$ refers to the smallest value of t_P from point $\mathbf{x}$ to any receiver n.

For each set of waveforms to be analysed, we perform a search over candidate event locations. For a candidate
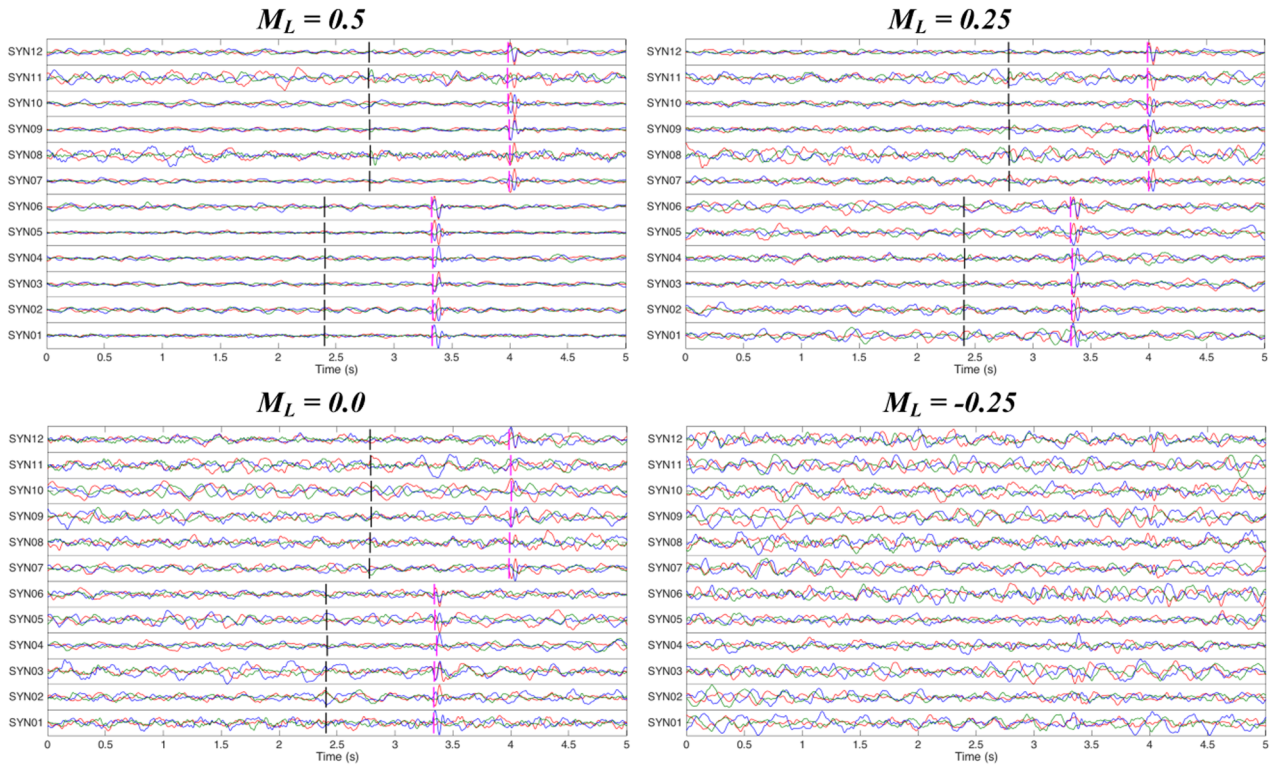
Figure 2 Synthetic waveforms used to assess the STA/LTA stacking algorithm using signals simulated by a finite-difference waveform simulation and noise from a temporary monitoring array deployed for baseline seismicity assessments prior to shale gas operations in the UK. (Red) North, (blue) east, and (green) vertical components are overlain for each receiver. The P– and S–wave arrival times based on the resulting hypocentre are shown by black and magenta ticks. The $M_L = 0.5$ event can be clearly seen above the noise levels, but as the event size is reduced, the arriving waveforms become harder to see above the noise and could easily be missed by auto-picking algorithms.

location **x**, we begin by rotating the horizontal components into a radial (S_V) and transverse (S_H) coordinate system using the geographical azimuth between the source and the receiver. For each component (V, S_H, S_V), we compute a running short-term/long-term average (STA/LTA) ratio based on the method described by Allen (1978). For each trace y, at time i, a characteristic function C is computed

$$C(i) = y(i)^2 + 3(y(i) - y(i-1))^2. \qquad (2)$$

The short- and long-time averages over sample lengths n_S and n_L are computed as

$$STA(i) = \frac{\sum_{j=i}^{i+n_S-1} C(j)}{n_S},$$

$$LTA(i) = \frac{\sum_{j=i-n_L}^{i-1} C(j)}{n_L}, \qquad (3)$$

and their ratio as

$$R(i) = STA(i)/LTA(i). \qquad (4)$$

For a given candidate event location **x**, the STA/LTA time series for each trace are time-shifted based on dt_P and dt_S. The aligned traces are then summed to create a stack

$$\Psi_v(\mathbf{x}, i) = \frac{\left[\sum_{k=1}^{n} R_v^k \left(i - \frac{dt_P(\mathbf{x},k)}{\delta} \right) \right]}{n},$$

$$\Psi_{S_H}(\mathbf{x}, i) = \frac{\left[\sum_{k=1}^{n} R_{S_H}^k \left(i - \frac{dt_{S_H}(\mathbf{x},k)}{\delta} \right) \right]}{n}, \qquad (5)$$

$$\Psi_{S_V}(\mathbf{x}, i) = \frac{\left[\sum_{k=1}^{n} R_{S_V}^k \left(i - \frac{dt_{S_V}(\mathbf{x},k)}{\delta} \right) \right]}{n},$$

where δ is the time-series sampling rate, and n is the total number of stations. The overall stack function is
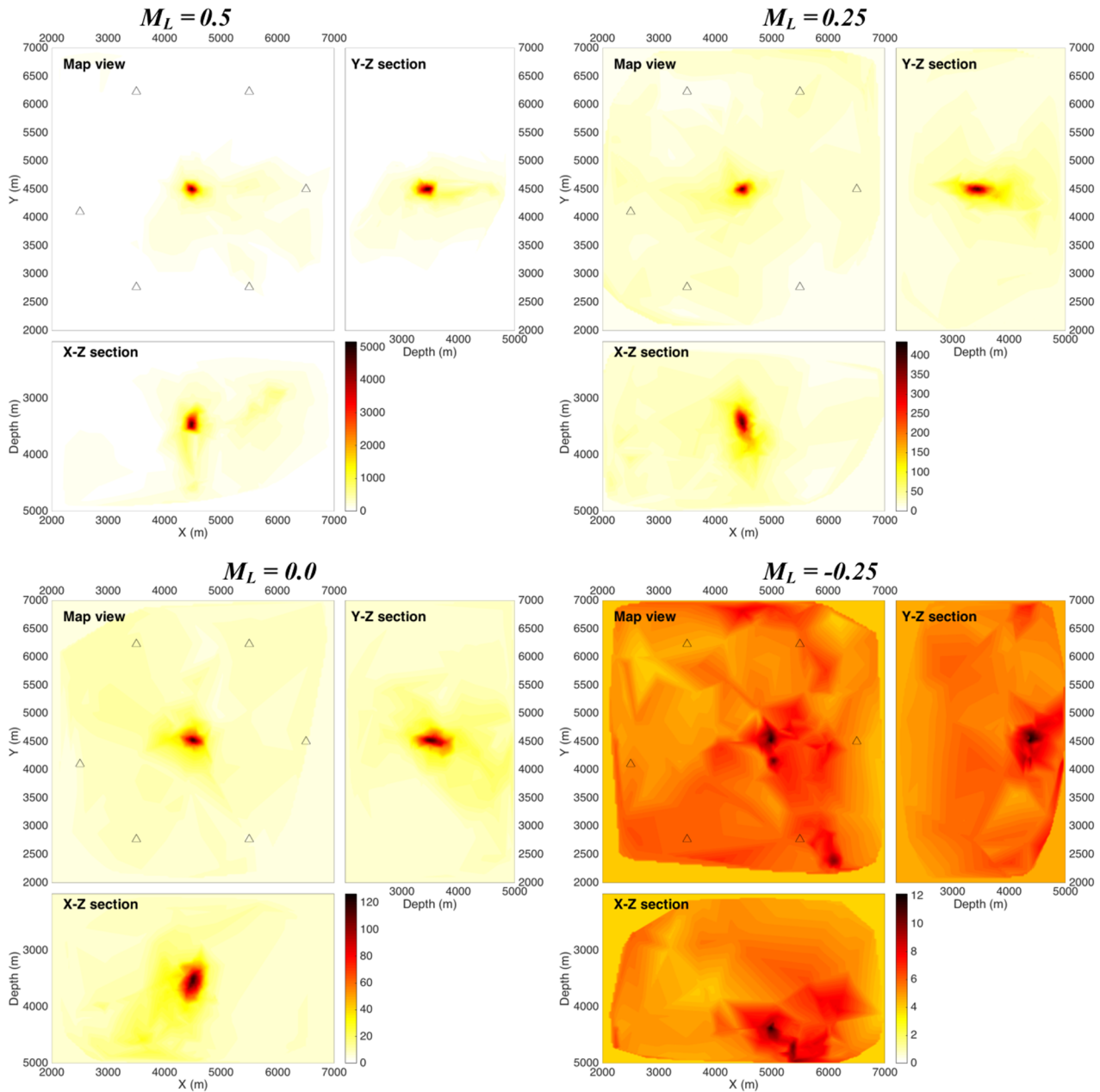
Figure 3 Map and cross-sectional slices through the $S'(\mathbf{x})$ volume for the different magnitude synthetic events. For the $M_L = 0.5$, 0.25, and 0.0 events, a clear maximum is found at the known event location ($\mathbf{x} = [4500\ 4500\ 3500]$). For the $M_L = -0.25$ event, local maxima are found that probably correspond to the spikes in the noise, but they are much smaller than the maxima from the true event locations. Note that the colour scale changes for each image.

determined from the product of the V, S_H, and S_V stacks

$$S(\mathbf{x}, i) = \Psi_v(\mathbf{x}, i)\Psi_{SH}(\mathbf{x}, i)\Psi_{SV}(\mathbf{x}, i). \quad (6)$$

The resulting stack function is a four-dimensional function of both spatial position and time. However, the function

can be simplified to take the maximum value at each spatial point within a given time window i to $i+\tau$

$$S'(\mathbf{x}) = \max(S(\mathbf{x}, \{i, \ldots, i + \tau\})), \quad (7)$$

reducing the results to a three-dimensional (3D) data cube (Chambers *et al.* 2010a).
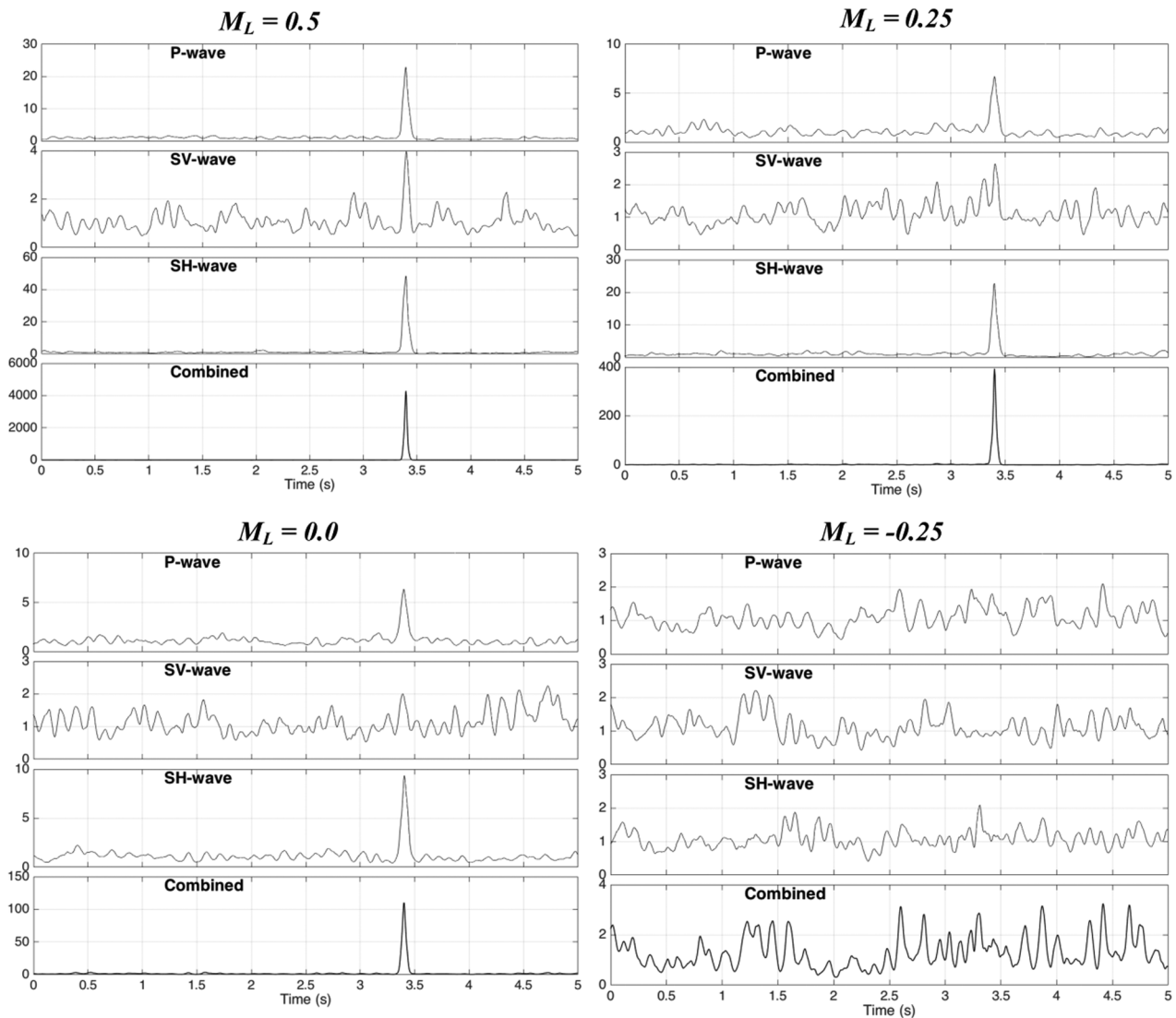
Figure 4 For each modelled event, we show the p–, s_V– and S_H–wave stacks, and the combined stack $S(\mathbf{x})$, which is the product of the stacks of the three phases. For the $M_L = 0.5$, 0.25, and 0.0 events, a clear peak is found at the expected event occurrence time. While peaks are found for the $M_L = -0.25$ event, they are far smaller and do not correspond to the event but to peaks found in the noise.

We note in passing that the ability of beamforming methods to focus an event in the correct position is dependent on the use of a correct velocity model and that an incorrect velocity model can affect the focusing power (and, hence, the ability to detect events). Chambers, Kendall and Barkved (2010b) examined the effect of velocity model inaccuracies on beamforming methods, finding that modest perturbations to a velocity model ($\pm 5\%$) affected the resulting depth position of the event but did not affect the focusing power of the image. Nevertheless, we stress the importance of using a well-calibrated model wherever possible. Velocity models at industrial sites can often be calibrated with other geophysi-

cal observations such as controlled-source reflection seismic imaging, sonic well logging; vertical seismic profiling; and by attempting to relocate string shots or other downhole sources whose position is known *a priori*.

2.2 Searching for events

Commonly, where beamforming-and-stacking-type event detection algorithms are used, a grid search is performed to find locations where the stack value exceeds a given threshold (e.g., Chambers *et al.* 2010a). This grid search over three spatial dimensions can be hugely expensive from a
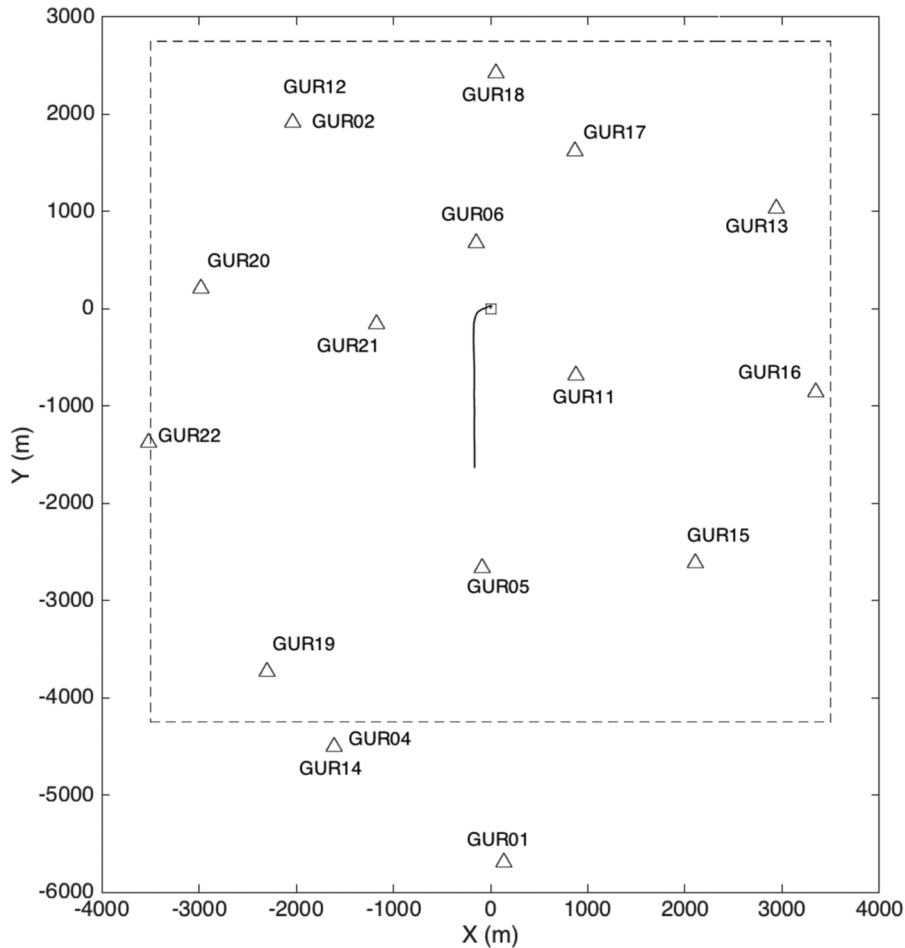
Figure 5 Monitoring setup for the case study. Surface broadband stations are marked by triangles, and the lateral extent of the treatment well is marked by the solid line. Note that stations GUR04 and GUR14, and GUR02 and GUR12, are co-located within a few metres of each other. The dashed square shows the bounds of the search for candidate event locations. The square shows the position of the well pad, with the track of one of the stimulated wells shown by the black line. The track of the other well is not marked, but it runs adjacent to the marked well.

computational point of view, making the use of such methods in real time a challenging proposition (though not impossible as long as sufficient computational power can be brought to bear). Instead, we seek alternative ways to search

the parameter space in order to reduce the computational cost.

We note that the stack power as a function of candidate position tends not to be particularly smooth: local maxima are common. Therefore, directional search algorithms are not

Table 2 FilterPicker parameters used to identify events. See Lomax *et al.* (2012) for full descriptions of these parameters

Parameter	Value
Sampling rate	200 Hz
T_{filter}	2s
T_{long}	10s
Threshold #1	10
Threshold #2	10
T_{UP}	20 samples

Table 3 One-dimensional layered velocity model used to locate events at the case study site

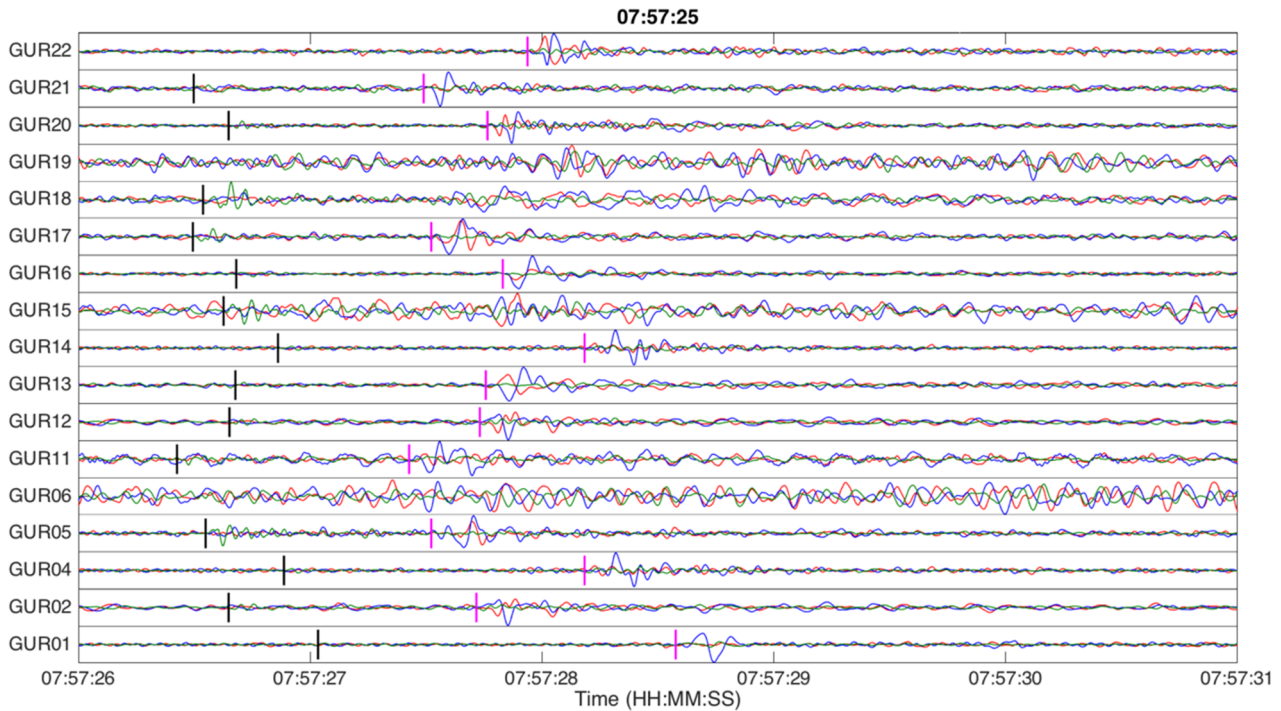| Depth to layer top (m)	V_P (m/s)	V_S (m/s)
0	3790	1930
400	3910	1990
900	4038	2060
4400	5230	2670
4900	5260	2680

Figure 6 Example event detected by the conventional automated picking algorithm (in the same format as in Fig. 2). Black and magenta ticks indicate the manually re-picked P– and S–wave arrivals. Data have been band-pass filtered between 1 Hz and 50 Hz.

appropriate as they tend to become trapped in these local maxima. Instead, global search algorithms are required. In this paper, we use the neighbourhood algorithm described by Sambridge (1999a) to search the parameter space. In the real example that follows below, we search for events within a volume of dimensions 3.5 km×3.5 km×3 km. We find that, where an event is present, a convergent maximum is found typically within 350 trial positions using the neighbourhood algorithm search method. Searching the same volume over a grid with 20-m spacing would entail over 4000000 trial positions, whereas even using 100-m spacing would entail over 30,000 trials. The improvements afforded by using the neighbourhood algorithm over a grid search, therefore reduc-

ing computational expense by orders of magnitude. Once a convergent maximum has been found, the imaging resolution can be appraised using Bayesian integration as described by Sambridge (1999b).

3 SYNTHETIC TESTS

Before applying it to a real example, we demonstrate our method using a synthetic dataset generated using the 3D finite-difference waveform-modelling package E3D (Larsen and Schultz 1995). We simulate a monitoring array of 12 seismometers with stations positioned in two concentric circles with radii of 2 and 4 km (Fig. 1), as might typically be used to monitor induced seismicity at an industrial site. We use a one-dimensional (1D) layered velocity model (listed in Table 1). In this case, we use an isotropic velocity model. The source is represented by a Ricker wavelet with a dominant frequency of 10 Hz. The model sampling rate is 200 Hz.

Waveforms are simulated from a strike-slip event at 3.5-km depth at the centre of this array ($\mathbf{x}$= [4500 4500 3500]). The amplitudes of the modelled waveforms are scaled such that they represent events with M_L of 0.5, 0.25, 0.0,

Table 4 Parameters used in the STA/LTA stacking algorithm applied to the case study site to search for events

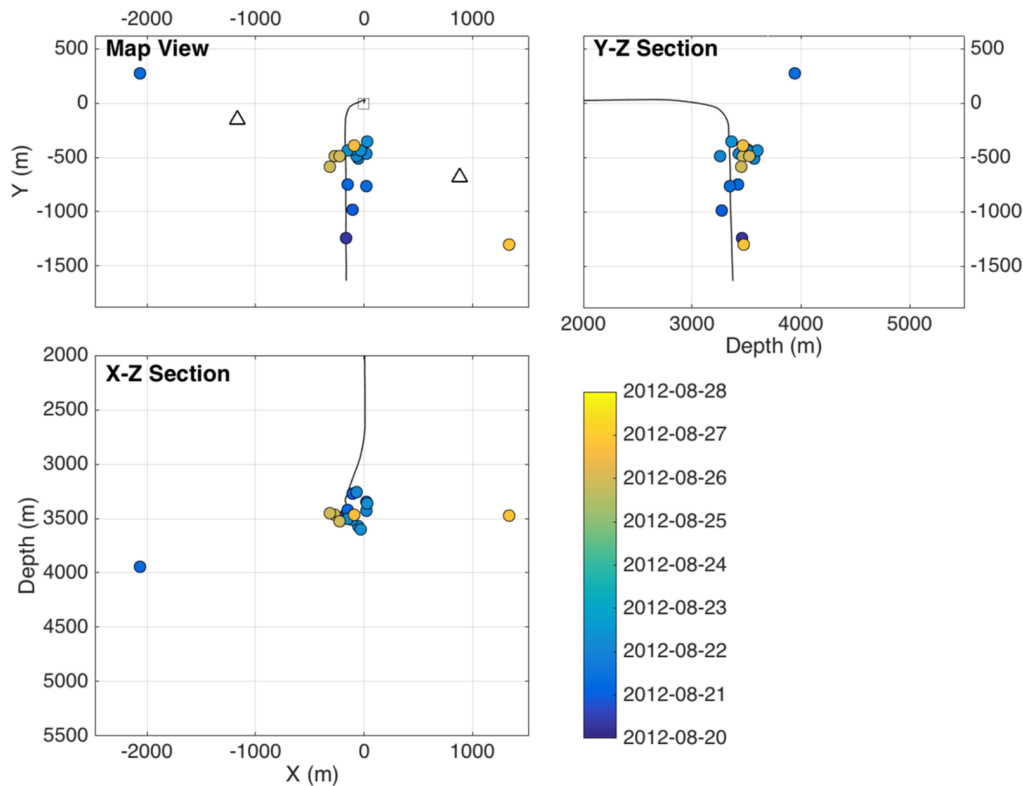| Parameter	Value
Sampling rate	200 Hz
Trace window length (τ)	30s
Short time window	10 samples
Long time window	200 samples
Band pass Filtering	1 – 50 Hz
Event candidate threshold	$S'(\mathbf{x}) > 15$

Figure 7 Map and cross-sectional views of the hypocentres of events detected using the conventional automated picking algorithm. These events were located by travel-time inversion of manually picked P– and S–wave arrivals. Events are coloured by their occurrence date.

and −0.25, as measured on the UK's local magnitude scale (Ottemöller and Sargeant 2013).

Synthetic data are often "contaminated" with noise derived from a statistical model (for example, Gaussian). However, doing so will not test the ability of our algorithm to detect events that are overlain on "real" ambient noise, which is often non-stationary and may be correlated across an array (Chambers *et al.* 2010a).

Instead, we overlay our modelled waveforms on real noise recorded by a temporary array of Güralp CMG-6TD broadband seismometers deployed in the northwest of England in an area in which shale gas exploration licenses have been awarded. The instruments were buried by hand to depths of approximately 0.5 m. This array was installed to provide baseline monitoring of shale gas operations in the UK. The use of real noise collected in the UK ensures that the noise is representative of conditions that might be expected when a TLS is in operation. Figure 2 shows the resulting waveforms, consisting of synthetic events superimposed on real noise.

For each synthetic event, we search over a 3D volume for maxima in $S'(\mathbf{x})$ that would indicate that an event is detected. Figure 3 shows slices through the $S'(\mathbf{x})$ volume for each

different event size, whereas Fig. 4 shows the stacks for the P–, S_H–, and S_V–waves. We find that, for the $M_L = 0.5$, 0.25, and 0.0 events, a clear maximum in $S'(\mathbf{x})$ is found that corresponds to the known position of the synthetic event. This peak is also apparent on the stacks of the individual waveforms, especially the P– and S_H–wave stacks, albeit less prominent on the S_V–wave stacks, as might be expected for the simulated strike-slip event. It is encouraging that the STA/LTA stacking algorithm is able to detect these events, as well as the $M_L = 0.0$ event in particular. This event is barely visible on the raw traces and may well be missed by commonly used automated picking algorithms that are based on identifying seismic waveform amplitude changes and even by manual analysis.

However, it is clear that the STA/LTA stacking algorithm has failed to detect the $M_L = -0.25$ event. Maxima in $S'(\mathbf{x})$ are found, but their amplitudes are substantially smaller than the amplitudes of the detected events, and there is more than one local maxima of similar amplitude. We surmise that these peaks are produced by the natural variability of the noise that we have superimposed. We use these observations to set a threshold for event detection in the following case study: we consider an event to have been detected when $S'(\mathbf{x}) > 15$. In
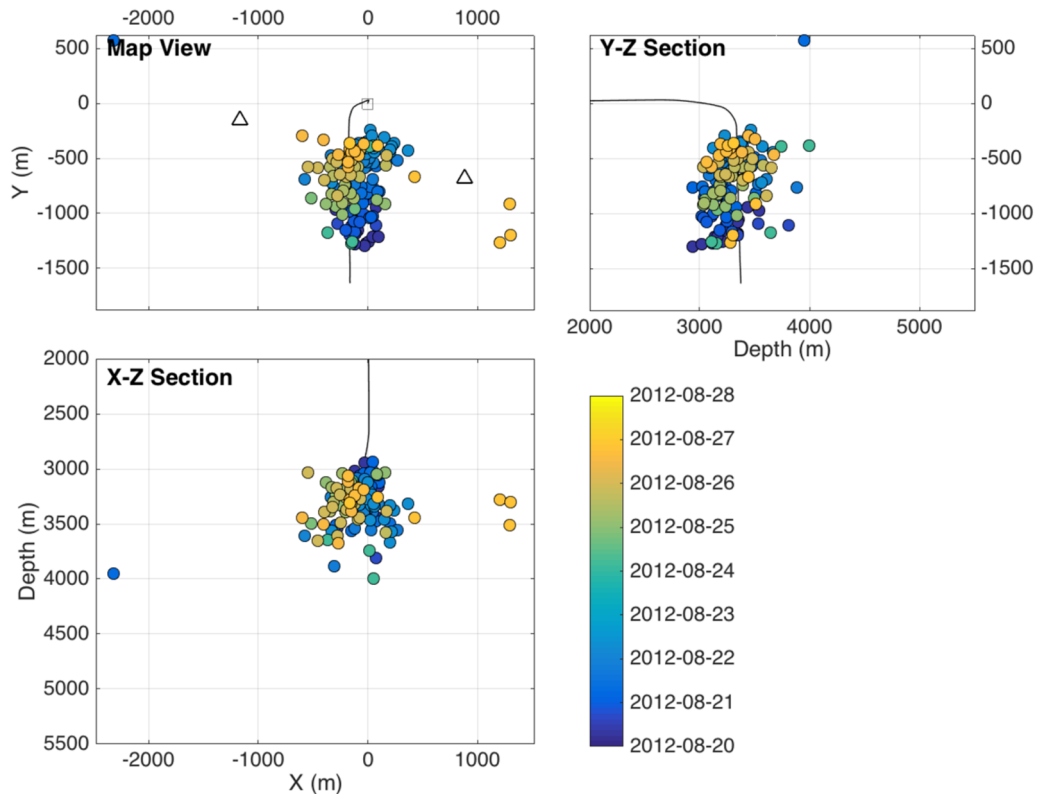
Figure 8 Map and cross-sectional views of the hypocentres of events detected and located by the STA/LTA stacking algorithm. Events are coloured by occurrence date.

practice, we envisage that an operator will set a threshold such that a suitable ratio of event detections versus false positives is achieved.

4 CASE STUDY

4.1 Description of monitoring site

Having demonstrated our method using a synthetic dataset, we now assess its performance monitoring a real-case study recorded during a multi-well, multi-stage hydraulic fracturing treatment in Oklahoma. The operations were monitored with an array of 17 three-component broadband Güralp CMG-3TD seismometers buried by hand to a depth of approximately 60 cm. The array geometry is shown in Fig. 5. The track of one of the horizontal wells is shown in this figure. The track of the second well was not made available to us by the operator, but it runs in the same direction adjacent to the marked well.

In this study, two horizontal wells were fractured sequentially over multiple stages. Monitoring was conducted continuously for 8 days. The target interval for the stimulation was

at a depth of approximately 3.8 km. Detailed engineering data (pumping times, rates, and pressures) were not made available to us by the operator.

4.2 Events detected using individual-trace automated phase picking methods

Prior to this study, the recorded data had been examined using commonly used seismological methods, where a triggering algorithm is used to identify potential event candidates, and travel-time picks are then inverted for event locations (e.g., Baptie 2012). Potential triggers were identified at each station using the *FilterPicker* automated picking algorithm described by Lomax *et al.* (2012) using the parameters listed in Table 2. *FilterPicker* is a commonly used automatic picking algorithm (e.g. Satriano *et al.* 2011; Utheim *et al.* 2014). Events were identified when triggers occurred simultaneously (within 3 seconds) on at least four stations. For these events, P– and S–wave arrivals were manually re-picked, and the phase arrival times were inverted for event locations.

The velocity model used to locate event is listed in Table 3. This velocity model was based on geophysical
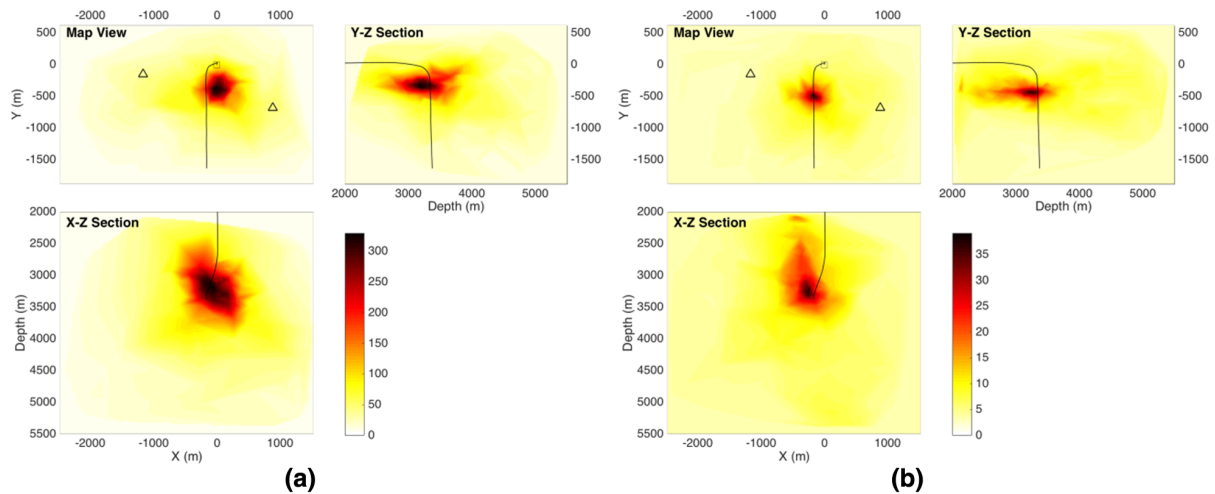
Figure 9 Slices through the volume of stack power ($S'(\mathbf{x})$) for an event with (a) good signal-to-noise ratio (i.e., detected by the conventional automated picking algorithm) and (b) weak signal-to-noise (i.e., undetected by the automated picking algorithm). The waveforms of the large event are shown in Fig. 6 and of the small event in Fig. 10.
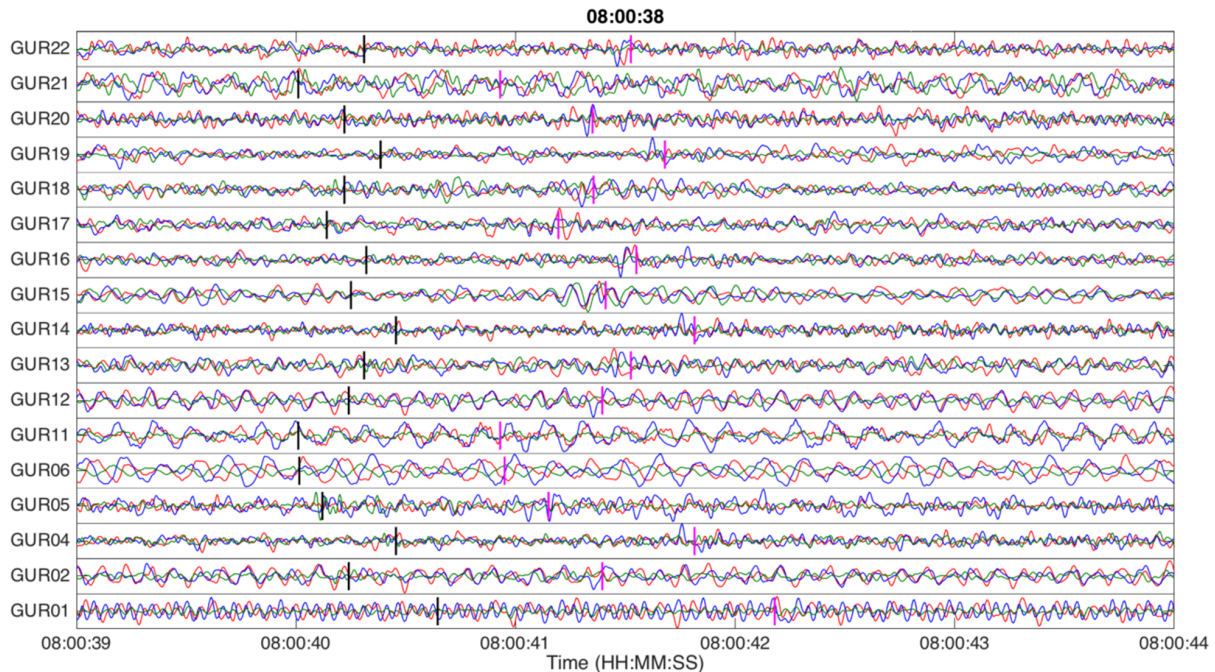

Figure 10 Example event detected by the STA/LTA stacking algorithm but missed by the automated picking algorithm (in the same format as in Fig. 2). The event is barely visible above the noise levels. Data have been band-pass filtered between 1 Hz and 50 Hz.

data (sonic well logs) provided by the site operator. These data did not contain any information about anisotropy, and we found that, in this case, an isotropic model was able to produce reasonable event locations with small residuals between observed and modelled pick times. We therefore decided to continue with an isotropic model for this case study. Moment magnitudes were computed using the method described by Stork, Verdon and Kendall (2014).

A total of 17 events were identified in this manner. Figure 6 shows the waveforms from an example event, and Fig. 7 shows the locations of the detected events. The events are clustered around the treatment wells and range in magnitude from approximately $0.0 < M_W < 1.0$.
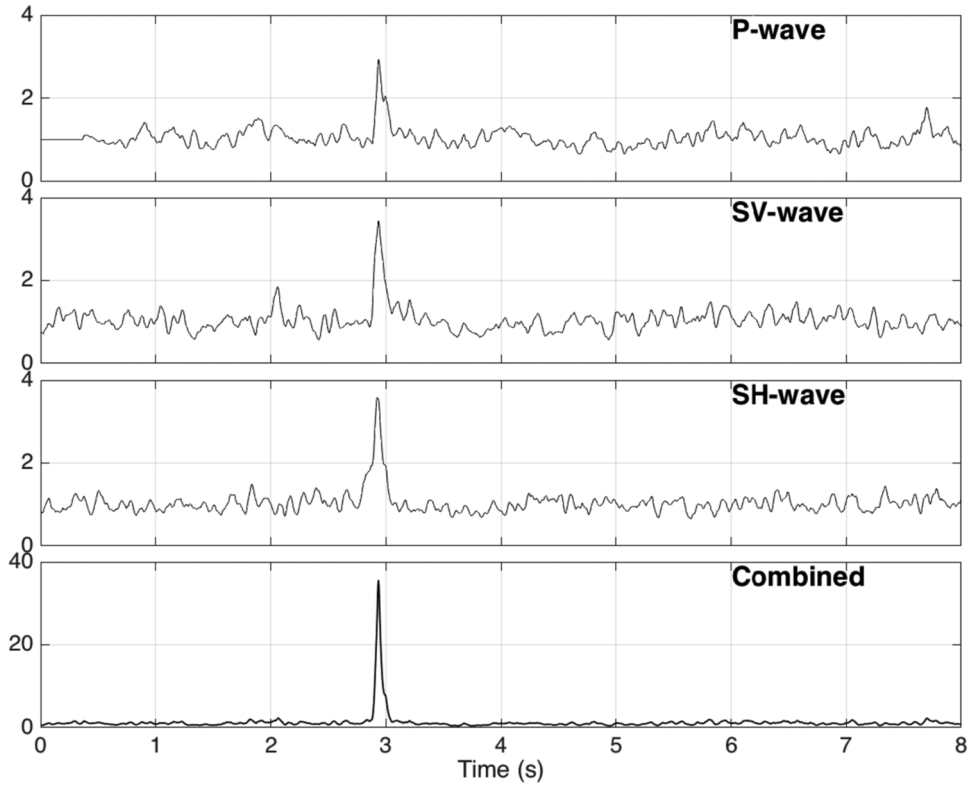
Figure 11 *P*–, S_H- and S_V-wave stacks, and the combined stack $S(\mathbf{x})$ for the best fit event location position for the weak event shown in Fig. 10. Small peaks in each of the individual phases combine to reveal a clear signal that is well above the noise on the combined trace.
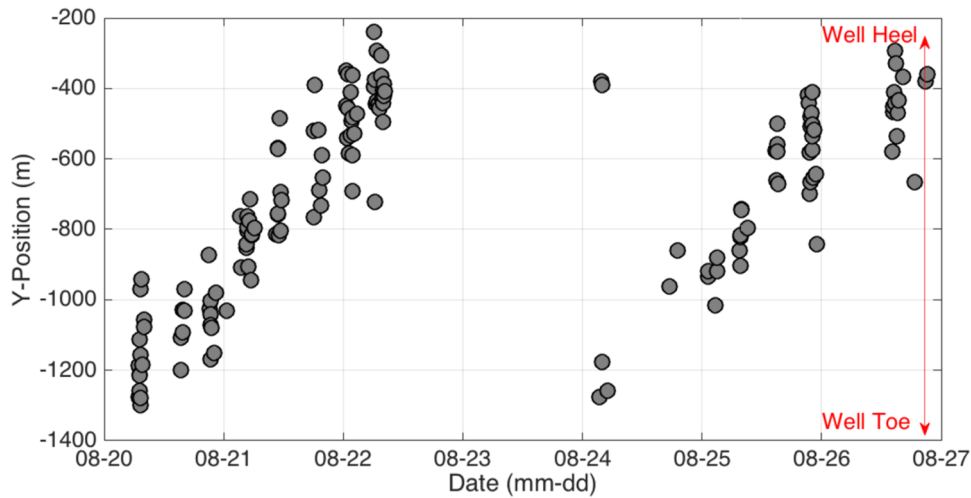

Figure 12 *Y*-coordinate position for each event as a function of occurrence time. Events move from the toes of the wells (at a position of approximately $Y \approx 1500$m) to the heels of the wells (at $Y \approx 0$ m), as expected for a typical hydraulic fracturing treatment program.

4.3 Events detected using short-term/long-term average stacking

The test for our method is to establish whether it can identify a larger number of events than detected by the automated picking algorithm. The parameters used for our search are listed in Table 4. As a preliminary processing step, the data are band-pass filtered with corner frequencies of 1–50 Hz. We set search limits to within a cube of 3.5 km×3.5 km×3 km around
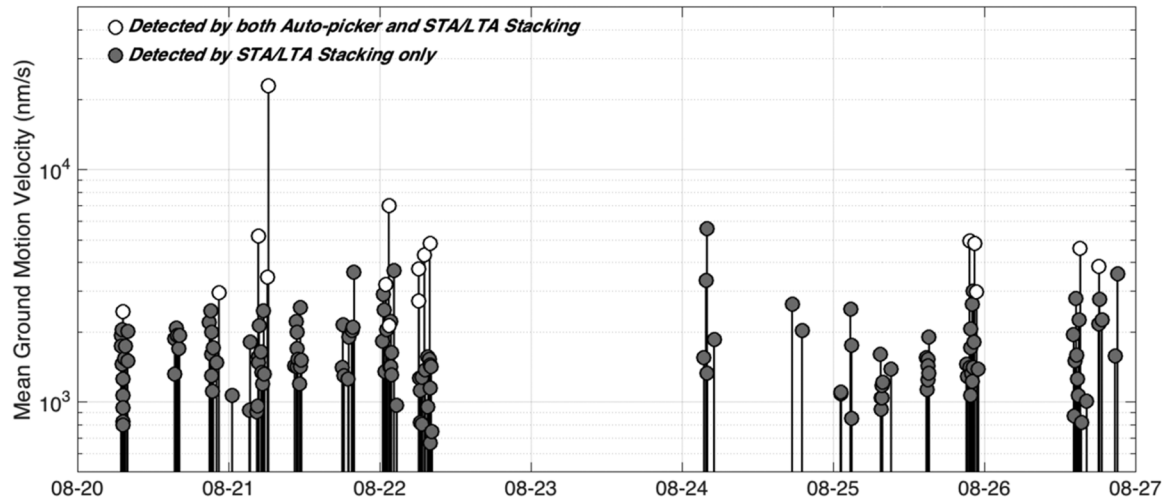
Figure 13 Mean PGV (over all 17 stations) for (white circles) events detected by the conventional auto-picking algorithm and (grey circles) events only detected by the stacking algorithm. The stacking algorithm is capable of detecting smaller events that are not identified by the auto-picking method.

the middle point of the horizontal section of the well. The lateral limits of our search are shown in Fig. 5 and between 2000-m and 5500-m depths. We divide the recorded data into time windows of $\tau = 30$ seconds, with 5 seconds of overlap between each segment. Within each 30-second segment, we search for candidate event locations. The velocity model we use is isotropic; hence, in this case, we compute a single S–wave travel-time table to shift both S_H and S_V phases. Based on the synthetic modelling described above, we set an event detection threshold whenever $S'(\mathbf{x}) > 15$. The event hypocentre is taken as the point $\mathbf{x}$ that maximises $S'(\mathbf{x})$.

A total of 155 events were detected and located over the 8-day monitoring period. This includes the 17 events detected using *FilterPicker* and represents a 900% increase in the number of events detected. The event locations are plotted in Fig. 8, coloured by the event occurrence date. Figure 9 shows slices through the stack power as a function of position for both a larger event (which was also detected by conventional picking, as shown in Fig. 6) and a smaller event, which initially went undetected. The waveforms from this smaller event are plotted in Fig. 10, and the individual P–, S_H–, and S_V–wave stacks (together with the combined stack) for this weak event are shown in Fig. 11.

In Fig. 8, we note that event locations migrate from the toe to the heel of the well with time. This behaviour is shown more explicitly in Fig. 12, which shows the Y-coordinate position of each event. We note two features from the figure. First, the events are clustered in time, with burst of events interspersed with quiescent periods. Unfortunately, the pumping

and engineering data for these wells are not available to us. Nevertheless, it seems likely that each burst of events corresponds to a fracturing stage in one of the wells, with seismicity being triggered during pumping and subsiding once pumping ceases.

Second, the progression of events from the toe to the heel of each well is immediately apparent. Normal hydraulic fracturing practice is to begin fracturing at the toe of each well, moving towards the heel of the well with each stage. In this case, the event positions track this behaviour, beginning at the toe of the first well and moving to the heel, before switching to the toe of the second well, and again moving towards the heel.

Because we do not have any engineering data from these operations, it is not possible to conduct any further analysis as to the implications of these events for the success (or otherwise) of the particular stimulation program. However, the fact that the timing and locations of the detected events are as expected, assuming a typical stimulation program, is encouraging as it provides further evidence that (i) the identified events are bona-fide low-signal-to-noise earthquakes and not artefacts co-incidentally generated by seismic noise and (ii) the event locations are sufficiently accurate to pick up the movement of the hydraulic fracture stages along the well.

4.4 Event sizes

In Fig. 13, we plot the mean peak ground velocity (PGV) amplitudes (mean over all stations for each event) for these events, based on windows around the anticipated S–wave

arrival times. In some cases, no clear S–wave arrival is visible above the noise levels on individual traces (as shown in Fig. 10). Therefore, the PGV in these cases is probably an overestimate because the measured value within some S–wave windows may in fact just be noise with a higher amplitude than the signal. The events detected by both the picking algorithm and by the stacking approach (white circles in Fig. 13) are generally the largest events in each stage, whereas those detected by the stacking algorithm only are generally smaller.

In the case study we have presented, we have examined PGV for events rather than computing event magnitudes. This is an intentional choice because, as discussed above, for the smaller events detected by the stacking algorithm, the amplitudes of phase arrivals on individual traces are similar to or sometimes below the noise levels. Stork *et al.* (2014) investigate the robustness of magnitude estimates for small-magnitude events and recommend that accurate magnitudes can only be calculated for events where the signal-to-noise ratio is 3 or greater. For most of the smaller events detected by the stacking algorithm, this criterion is not met; hence, we have not attempted to determine magnitudes for these smaller events since they would be subject to substantial error. While it is possible to compute event magnitudes based on stacked waveforms, in our experience, magnitudes estimated via this type of approach may not be particularly robust.

5 CONCLUSIONS

In order to detect and identify induced seismic events at industrial sites such as shale gas extraction wells, operators are increasingly using small, sparse arrays of surface seismometers. Such arrays have the advantage of cheapness and ease of deployment over the downhole arrays and/or dense surface arrays commonly used to image microseismic activity. To maximise the information that can be gained from these arrays, the detection thresholds must be minimised. This can be challenging in high-noise environments that often exist around industrial sites.

To improve detection thresholds of small, sparse, surface arrays, we develop and test a method that uses beamforming and stacking of characteristic functions based on short-term/long-term average (STA/LTA) ratios to detect events that have signal-to-noise ratios close to 1. In this paper, we apply this approach to data recorded during hydraulic fracturing of a well in Oklahoma. Our aim was to compare the performance of this approach to typically used event detection algorithms that rely on automated phase picking on individual traces.

We find that, by using this beamforming-and-stacking approach, we were able to substantially increase the number of events detected. Where a conventional picking algorithm was only able to detect 17 events during the monitoring period, the beamforming-and-stacking approach was able to detect 155 events. Generally speaking, the signal-to-noise ratio of these additional events was close to 1, and they could easily have been missed even by manual analysis of the recorded waveforms.

The hypocentres of the detected events are close to the wellbore and follow a pattern expected for a typical hydraulic stimulation program. The events occur in bursts, followed by quiescent periods, which we infer that they correlate to the hydraulic fracturing stages (although we do not have the pumping data available to confirm this), and with each stage, move from the toe to the heel of the well.

We conclude that the STA/LTA stacking algorithm has been successful in detecting small-magnitude events that could not be detected with more conventional methods and that, in addition these, small events have been accurately located. We recommend that algorithms of this nature be used at future industrial sites to maximise the information that can be provided by small, sparse, surface seismometer arrays.

REFERENCES

Allen R.V. 1978. Automatic earthquake recognition and timing from single traces. *Bulletin of the Seismological Society of America* **68**, 1521–1532.

Baptie B. 2012. Earthquake Monitoring 2011/2012. British Geological Survey Commissioned Report OR/12/092.

BC Oil and Gas Commission. 2012. Investigation of Observed Seismicity in the Horn River Basin. Accessed from http://www.bcogc.ca/node/8046/download on 23 July 2015.

BC Oil and Gas Commission. 2014. Investigation of Observed Seismicity in the Montney Trend. Accessed from https://www.bcogc.ca/node/12291/download on 23 July 2015.

Chambers K., Kendall J.-M., Brandsberg-Dahl S. and Rueda J. 2010a. Testing the ability of surface arrays to monitor microseismic activity. *Geophysical Prospecting* **58**, 821–830.

Chambers K., Kendall J.-M. and Barkved O. 2010b. Investigation of induced microseismicity at Valhall using the Life of Field Seismic array. *The Leading Edge* **29**, 290–295.

Clarke H., Eisner L., Styles P. and Turner P. 2014. Felt seismicity associated with shale gas hydraulic fracturing: the first documented example in Europe. *Geophysical Research Letters* **41**, 8308–8314.

Darold A., Holland A.A., Chen C. and Youngblood A. 2014. Preliminary analysis of seismicity near Eagleton 1-29, Carter County, July 2014. Oklahoma Geological Society Open File Report, OF2-2014.

Duncan P.M. and Eisner L. 2010. Reservoir characterization using surface microseismic monitoring. *Geophysics* **75**, A139–A146.

Eisner L., Zhang Y., Duncan P., Mueller M.C., Thornton M.P. and Gei D. 2011. Effective VTI anisotropy for consistent monitoring of microseismic events. *The Leading Edge* **30**, 772–776.

Grechka V. 2015. Tilted TI models in surface microseismic monitoring. *Geophysics* **80**, WC11–WC23.

Green C.A., Styles P. and Baptie B.J. 2012. Preese Hall shale gas fracturing, review and recommendations for induced seismic mitigation. Department of Energy and Climate Change. Accessed from https://www.gov.uk/government/uploads/system/uploads/attachment_data/file/15745/5075-preese-hall-shale-gas-fracturing-review.pdf on 23 July 2015.

Grigoli F., Cesca S., Amoroso O., Emolo A., Zollo A. and Dahm T. 2014. Automated seismic event location by waveform coherence analysis. *Geophysical Journal International* **196**, 1742–1753.

Guest W.S. and Kendall J.-M. 1993. Modelling waveforms in anisotropic inhomogeneous media using ray and Maslov asymptotic theory: applications to exploration seismology. *Canadian Journal of Exploration Geophysics* **29**, 78–92.

Horleston A., Stork A., Verdon J., Baird A., Wookey J. and Kendall M. 2013. Seismic monitoring of drilling operations in Balcombe, West Sussex. University of Bristol. Accessed from http://www1.gly.bris.ac.uk/BUMPS/PDFS/BristolBalcombeReport2013.pdf on 23 July 2015.

Fomel S. 2004. On anelliptic approximations for qP velocities in VTI media. *Geophysical Prospecting* **52**, 247–259.

Friberg P.A., Besana-Ostman G.M. and Dricker I. 2014. Characterisation of an earthquake sequence triggered by hydraulic fracturing in Harrison County, Ohio. *Seismological Research Letters* **85**, 1295–1307.

Kendall J.-M., Fisher Q.J., Covey Crump S., Maddock J., Carter A., Hall S.A. *et al.* 2007. Seismic anisotropy as an indicator of reservoir quality in siliciclastic rocks. In: *Structurally Complex Reservoirs* (eds S.J. Jolley, D. Barr, J.J. Walsh and R.J. Knipe). *Geological Society of London Special Publications* **292**, 123–136.

Larsen S. and Schultz C.A. 1995. ELAS3D: 2D/3D elastic finite-difference wave propagation code. Technical Report UCRL-MA-121792, 1–19.

Lomax A., Satriano C. and Vassallo M. 2012. Automatic picker developments and optimization: FilterPicker—A robust, broadband picker for real-time seismic monitoring and earthquake early warning. *Seismological Research Letters* **83**, 531–540.

Maxwell S.C., Rutledge J., Jones R. and Fehler M. 2010. Petroleum reservoir characterization using downhole microseismic monitoring. *Geophysics* **75**, 75A129–75A137.

National Research Council. 2013. *Induced Seismicity Potential in Energy Technologies*. Washington, DC: The National Academies Press.

Ottemöller L. and Sargeant S. 2013. A local magnitude scale M_L for the United Kingdom. *Bulletin of the Seismological Society of America* **103**, 2884–2893.

Sambridge M. 1999a. Geophysical inversion with a neighbourhood algorithm—I. Searching a parameter space. *Geophysical Journal International* **138**, 479–494.

Sambridge M. 1999b. Geophysical inversion with a neighbourhood algorithm—II. Appraising the ensemble. *Geophysical Journal International* **138**, 727–746.

Satriano C., Elia L., Martino C., Lancieri M., Zollo A. and Iannaccone G. 2011. PRESTo, the earthquake early-warning system for southern Italy: concepts, capabilities and future perspectives. *Soil Dynamics and Earthquake Engineering* **31**, 137–153.

Schulz R., Mei S., Pana D., Stern V., Gu Y.J., Kim A. *et al.* 2015. The Cardston earthquake swarm and hydraulic fracturing of the Exshaw Formation (Alberta Bakken play). *Bulletin of the Seismological Society of America* **105**, 2871–2884.

Skoumal R.J., Brudzinski M.R. and Currie B.S. 2015. Induced earthquakes during hydraulic fracturing in Poland Township, Ohio. *Bulletin of the Seismological Society of America* **105**, 189–197.

Stork A.L., Verdon J.P. and Kendall J.-M. 2014. The robustness of seismic moment and magnitudes estimated using spectral analysis. *Geophysical Prospecting* **62**, 862–878.

Utheim T., Havskov J., Ozyazicioglu M., Rodriguez J. and Talavera E. 2014. RTQUAKE, A real-time earthquake detection system integrated with SEISAN. *Seismological Research Letters* **85**, 735–742.

Verdon J.P. and Kendall J.-M. 2015. Written Evidence submitted to the Commons Select Environmental Audit Committee Inquiry on the Environmental Risks of Fracking. FRA0022. Accessed from http://data.parliament.uk/writtenevidence/committeeevidence.svc/evidencedocument/environmental-audit-committee/environmental-risks-of-fracking/written/17012.pdf on 23 July 2015.

Wang Z. and Krupnick A. 2013. A retrospective review of shale gas development in the United States: What lead to the boom? *Resources for the Future DP* 12–13.